Interferometer study of radial and axial density evolution and temperature in N_2 gas subjected to negative and positive corona discharges

M. Lemerini[a], A. K. Ferouani[a,b] and M. Sahlaoui[a,b]

[a]*L.P.T Laboratory, Department of Physics, Faculty of Sciences, University of Tlemcen, 13000 Tlemcen, Algeria.*
[b]*Ecole Supérieure en Sciences Appliquées, BP 165 RP Bel Horizon, Tlemcen 13000, Algeria.*
E−mail: mostefa.lemerini@gmail.com and ferouani_karim@yahoo.fr

Received 10 February 2023; accepted 19 September 2023

In the present paper, we propose to make an optical diagnosis by laser interferometry to determine experimentally the density of neutral particles in a coronal discharge bathing in a gaseous medium N_2. We are particularly interested in the measurement of variation of the optical path and therefore of the index of refraction which allows us to highlight the variation of the density of the neutrals in the discharge, and using a computer treatment (Pearce method) the refractive index of the medium is calculated to determine the spatial distribution of density and temperature (radial and axial) at the core of the corona discharge in two different situations (positive and negative). This optical diagnosis also allowed us to quantitatively determine the phenomenon of depopulation of neutral particles. These quantitative and experimental results are interesting because they allow a good correlation between the theoretical results obtained so far.

Keywords: Corona discharge; Pearce method; Abel inversion; Gladstone−Dale equation; Mach−Zehnder interferometer.

DOI: https://doi.org/10.31349/RevMexFis.70.021302

1. Introduction

Numerous studies have been written on the issue of negative and positive corona dicharge, which has been studied for a very long time. The temperature and the density of the neutral gas changes spatially and temporally when the plasma and neutral molecular energy interact during the formation and growth of the plasma in a point to plane gas discharge (see *e.g.* [1, 2]). The corona discharge is part of the family of non thermal cold plasmas and it is usually used at atmospheric pressure. It is always associated with two electrodes, one to a small radius of curvature is subjected to a high voltage, and the other electrode has a radius much larger. The polarity depends on the nature of the voltage applied to the electrode with a small radius of curvature. There are numerous industrial uses for electrostatic precipitation [3], environmental cleanup techniques [4], ozone production [5]. Both theoretical research [6, 7] and practical studies [8, 9] have demonstrated the central role of neutral heating in the initiation of gas breakdown. Optical and electrical analyses of the behavior of a point to plane discharge for centimeter sized air gaps at atmospheric pressure.

Therefore, by examining the impacts that come from various physical processes, we could complete the plasma diagnostics. Measurements of gas evolution in plasma have been made using Raman scattering techniques, sound, ultrasonic velocity electromagnetic wave probing, infrared spectra, and absorption spectra. Since these interferometry techniques often measure the optical path through the medium, we can infer the refractive index, density, and temperature from the relationship between these factors [8].

In investigations of fluid flow, combustion, heat transfer, plasmas, and diffusion, interferometry is frequently employed because local fluctuations in the refractive index can be connected to changes in pressure, temperature, or the relative concentration of various components. For such investigations, the Mach−Zehnder (M−Z) interferometer is frequently employed [10]. Microscopy is a significant area in which optical interferometry is used. When stylus profiling cannot be utilized due to the risk of damage, interference microscopy offers a noncontact way for analyzing the structure and estimating the roughness of specular surfaces [11].

Many cutting-edge optical techniques have recently been created to estimate the temperature of such an object. B.H. Lee *et al*. [12] employed fiber optic interferometers to measure pressure, temperature, strain, and refractive index, among other physical variables. They elaborated on a few specific interferometeric sensor application examples and demonstrated their enormous potential for real-world use.

P. Lu *et al*. [13] used a M−Z interferometer to detect the temperature and the refractive index simultaneously. They demonstrated how temperature and variations in the environment's refractive index affect the wavelength of the peak attenuation of interference with a particular sequence in the transmission spectrum.

Yet, it is quite intriguing to investigate the phenomenon between ion gas and neutral gas by using the corona discharge with the M−Z interferometer. The experimental setup of point to plane at high voltage is the foundation for the research of this phenomenon [8].

In the present study, the M−Z interferometry method is successfully developed to analyse and diagnose a N_2 gas medium subjected to a point to plane type corona discharge in two situations different positive and negative polarity. The interferograms are captured using a CCD Camera (see Fig. 2), and the inverse Abel transformation ensures that they may be

numerically analyzed. We want to deduce mainly the mapping of the refraction index, the radial and axial variation of the density and the temperature of the neutral particles.

2. Experimental set-up

The laser beam (wavelength $\lambda = 0.6328\ \mu$m) is collimated to have a plane wavefront into the M−Z interferometer, and the beam inside the interferometer is separated by a beam splitter and later on the two beams are combined with another beam splitter, see Fig. 1. The electrodes are, moreover, visible on the interferogram, the interelectrode distance d is measured using a pattern. The gas discharge image is recorded with a Camera placed at the outlet of the interferometer. The pressure of the N_2 bottle is measured with a regulator. A mathematical treatment allows us to extract directly, from the interferogram, a mapping of the phase variation introduced by the coronal discharge. Abel's inversion is now an integral part of this program and allows us to have directly the gas density profiles.

The various essential elements for the M−Z interferometer are given in Fig. 2. Our discharge system consists of two electrodes point to plane, made of stainless steel. The radius of curvature of the point is 100 μm and the diameter of the plane is 25 mm. To power these systems, we have a high voltage generator with a voltage of 35 kV. This generator is connected to the discharge via a resistance of $20 \times 10^6\ \Omega$. First, it is necessary to obtain the fringes without applying the discharge. Second stage: high voltage is supplied to the point electrode (corona discharge). Due to the discharge's density gradient and the light's path's disruption of the gas distribution in space, the fringes are deformed. The map of the density, temperature, and refractive index of the N_2 gas is then determined by measuring the difference between these two interferograms.

FIGURE 1. Overview of the experimental set-up.

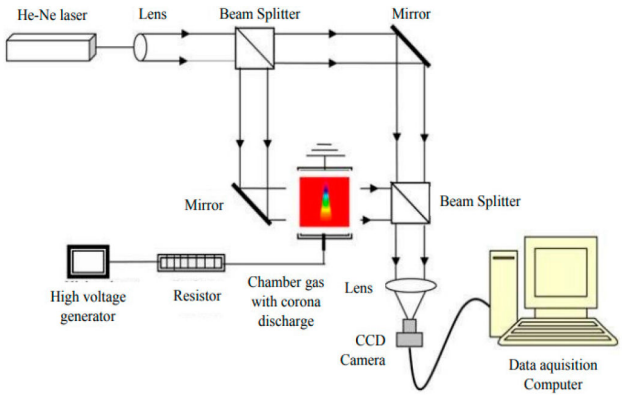

FIGURE 2. Experimental device of the interferometric system.

3. The finite fringe interferometric method

This method is based on analysis of interferograms which were obtained and recorded from a screen by CCD camera illustrated in Fig. 2. So, the intensity of the interference pattern, for each interferogram can be written as follows [14,15]:

$$I(z,r) = a_0^2 + a_i^2 + 2\,a_0\,a_i\,\cos\left(\Delta\phi(z,r)\right), \qquad (1)$$

where $I(z,r)$ indicates the light's intensity at the axial z and radial r point, a_0 is the intensity of the beam crossing the chamber, and ai the intensity of the reference beam (see Fig. 2). The last term $2\,a_0\,a_i\,\cos\left(\Delta\phi(z,r)\right)$ means the interference term, and it depends on the phase difference $\Delta\phi$.

The phase information of a light wave that originates from a coherent light source changes when it travels through a corona discharge because the discharge's refractive index changes. We must first determine the refractive index using the Abel inversion and Pearce method approach in order to calculate the density (more details of the refractive index can be found in Refs. [8, 16, 17]). In this method:

$$d\,k(z,r) = \frac{2}{\lambda}\int_r^R \frac{N(z,r)r'}{(r'^2 - r^2)^{\frac{1}{2}}}\,d\,r', \qquad (2)$$

where $k(z,r)$ denotes the phase shifting at position (z,r), λ is the wavelength of the laser used, $N(z,r)$ is the refractive index along the ray path through the discharge, R is the study ray and r' is the discharge ray. The integration occurs along the path that the object beam follows through the discharge.

The index variation responds to changes in neutral density. The Gladstone−Dale relation in our situation enables us to determine the refractive index of neutral particles, can be expressed as [8]:

$$N - 1 = N_n\left[\chi_n\,(1-\xi) + \chi_i\,\xi\right] + \chi_e\,N_e, \qquad (3)$$

where N being the index of refraction of the medium, N_n is the density of the neutral particles, N_e is the density of the electrons, ξ is the degree of ionization and χ_n, χ_i, χ_e are the Gladstone constants, corresponding, respectively, to the population of the neutrals, ions and electrons. It is worth mentioning that in a weakly ionized gas, as in the case of the plasma created by the corona discharge, the degree of ionization is negligible. Thus, the only factor affecting the optical properties of light pencils is the density of neutral

species. The Gladstone-Dale relationship, defined by M. Lemerini [8]:

$$N - 1 = \varrho\, \chi_g, \tag{4}$$

where ϱ is the mass density and χ_g ($= 1.97 \times 10^{-4}$ in $m^3\,kg^{-1}$) is the Gladstone coefficient.

It should be mentioned here that Eq. (4) can also be written with wavelength λ, dephasing $\Delta\Phi$ between the fringes, and length L of the path of the beam inside the disturbed medium, as:

$$N - 1 = \frac{\lambda\,\Delta\Phi}{2\,\pi\,L}. \tag{5}$$

The index of refraction of the medium is determined by applying Eq. (5), the density of neutral species N_N is calculated from Eq. (4), and the ideal gas law is then used to get the temperature of the gas, by the well-known equation [8, 18]:

$$\theta = \theta_0 \left[\frac{p\,(N_0 - 1)}{p_0(N - 1)}\right], \tag{6}$$

where, θ is the dependence of the temperature distribution on each point, θ_0 (= 300 in Kelvin) is the room-temperature N_0 is the reference refractive index of the ambient, p is the pressure of the gas and p_0 (= 1 in atm) is the reference room-pressure.

4. Results and discussions

In a radially symmetric system, we take into account two parallel electrodes that point to plane (z, r), where z is the distance that varies between the point to plane (the point is situated at $z = 0$ and the plane at $z = 10$ mm), where r is the distance that varies between the discharge axis and the lateral ends ($r = 0$ means the point to plane axis and $r = 2.5$ mm means the lateral limit of the point discharge).

The results obtained with the interferometer described above concerning N_2 gas are given in Fig. 3, and they show respectively the interferogram without and with corona discharge.

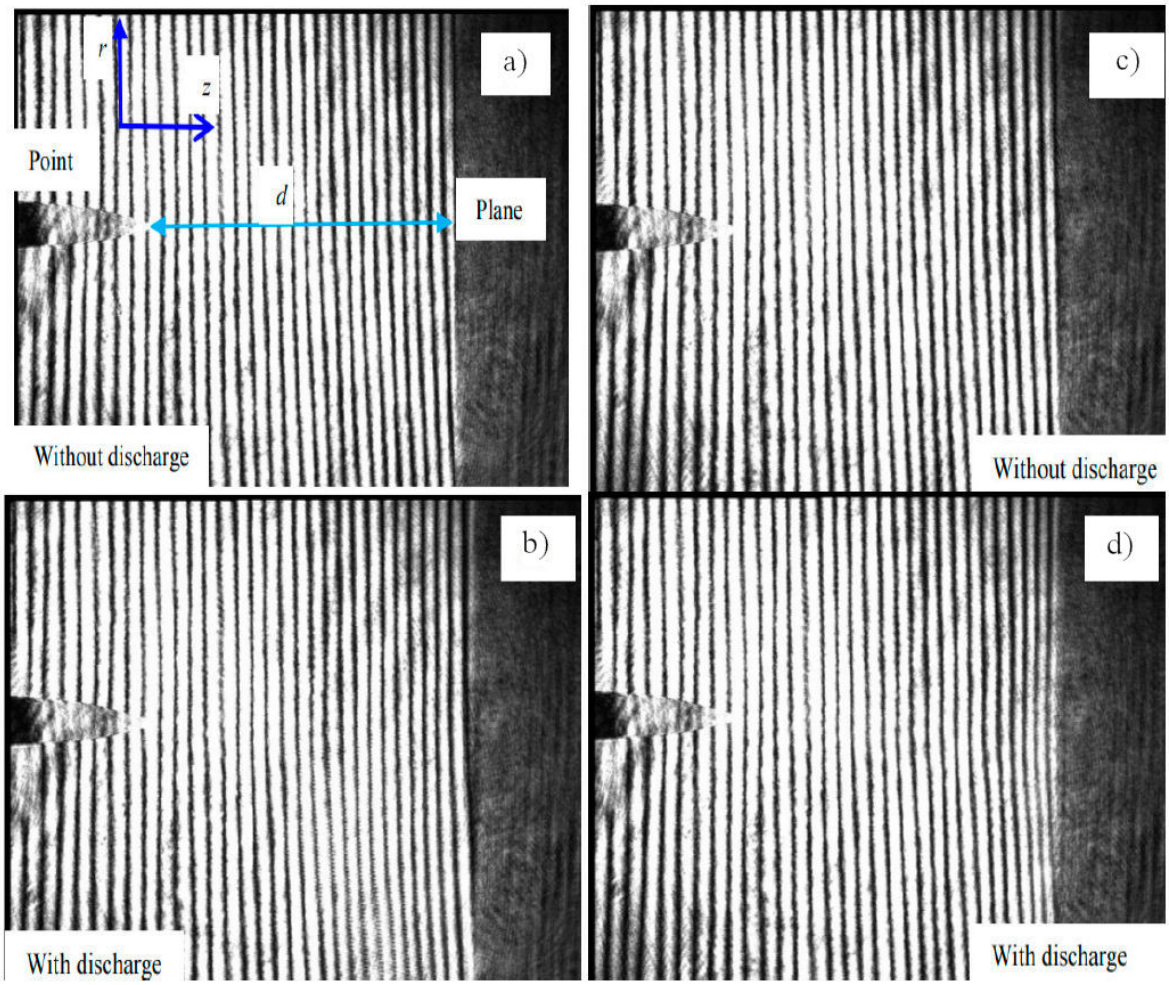

FIGURE 3. Interference fringes obtained with and without corona discharge, of N_2 gas (interelectrode $d = 10$ mm, pressure $p_0 = 1$ atm and temperature $T_0 = 300$ Kelvin). At left a), b): case of positive polarity. At right c), d): case of negative polarity.

The interferograms obtained show deformed fringes in the cone of discharge between the point and plane. The meaning is therefore that the polarity of the deformation of these fringes is arbitrary, it depends on the experimental situation and the expected results. Given the previous observations, we know that the crown discharge must present at its center a decrease in the density of neutral particles. The deformation of the fringes must therefore lead us to a decrease in the refractive index.

We clearly observe in Fig. 3b), that there is a more nuanced distribution in all the volume occupied by the gas. Indeed, the transfer of motion between neutral particles becomes very important and the influence of charged particles also increases especially in the middle and near the point. We can also note in Fig. 3d) the cone of the discharge that propagates towards the plane because the pressure exerted on the neutrals becomes important. It can also be noticed in Fig. 3d) the movement of neutral particles diffuses towards the side walls of the discharge along the cathode due always to the transfer of energy neutral gas/charged particles.

4.1. Spatial evolution of the neutral population

We will now examine the sensitivity of corona discharge on the density neutrals. In Fig. 4, we show the evolution of the density of the neutrals along the axis of the discharge, for two types of corona discharge (negative and positive). We observe on these two curves that depopulation is more important in the vicinity of the plane than near the point, or more precisely, at for example, in which axial distance $z = 9$ mm from the point. Indeed, values of the density ranging from $\sim 1.6\times10^{19}$ molecules/cm^3 for positive discharge, representing a depopulation rate of 76% and $\sim 1.8 \times 10^{19}$ molecules/cm^3 for negative discharge, representing a depopulation rate of 68%. On the other hand, near the peak there are values of the density $\sim 1.85 \times 10^{19}$ molecules/cm^3 for positive discharge representing a population rate of 26%), to $\sim 2.0 \times 10^{19}$ for negative discharge (representing a population rate of 18%).

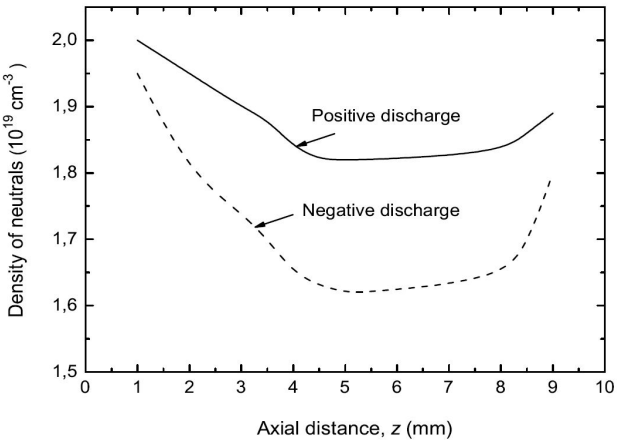

FIGURE 4. Axial evolution of neutral density of gas N_2 subjected to a negative and positive corona discharge.

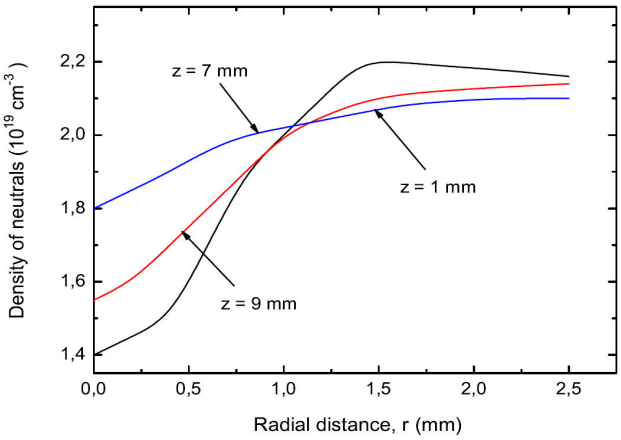

FIGURE 5. Radial evolution of neutral density of gas N_2 subjected to a positive corona discharge.

It is clear from these results that the dynamics of the neutrals are greater at a distance equal to one third of the inter-electrode distance close to the plane. It is in this area that heat transfers and collisions between particles occur with greater intensity than in the vicinity of the electrodes.

In Fig. 5, we plot the radial evolution of the neutral density for the positive corona discharge for three selected values of z axial distance, *i.e.* $z = 1$ mm (near the point), z= 7 mm (third of the inter-electrode distance) and $z = 9$ mm (near the plane). From Fig. 5 we can identify two regions: a region that extends between $r = 0$ and $r = 1.6$ mm, in which the density of the molecules is less than the density of the ambient air whatever the position between the point and the plane. The second region of these curves, that is to say for $r \gtrsim 1.6$ mm or at the edge of the discharge, indicates a higher population density than that of the ambient air.

We also observe on these curves that the relative rate of depopulation for the three selected points is different. Indeed, for the vicinity of the point ($z = 1$ mm) we note values ranging from 12 to 23% for $r \lesssim 1.6$ mm, while for this same radial distance and for z = 9 mm we have values varying from ∼70 to 35% and for $z = 7$ mm we have ~ 44 to 23%.

In the same way Fig. 6 presents our results for the evolution of the radial neutral density for the negative discharge. We distinguish two distinct regions: First, the low radial distance $0 \leq r \leq 1.9$ mm in which the density of the molecules is less than the density of the ambient air whatever the position between the point and the plane. The second region is for $r \gtrsim 2$ mm. We also observe from these curves that the relative rate of depopulation for the three chosen points is different. Indeed, in the vicinity of the point (*i.e* $z = 1$ mm) we note values ranging from 9 to $\sim 25\%$ for $r \leq 2$ mm, while for this same radial distance and for $z = 9$ mm we have values varying from ~ 30 to 47% and for $z = 7$ mm we have ~ 15 to 22%.

It is also interesting to note this radial evolution. We can divide each curve of the Figs. 5-6 from the centre of the discharge outward, in three parts: a relatively small part where the

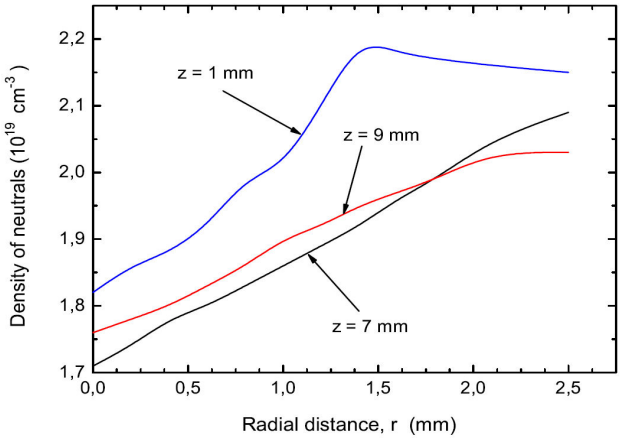

FIGURE 6. Radial evolution of neutral density of gas N_2 subjected to a negative corona discharge.

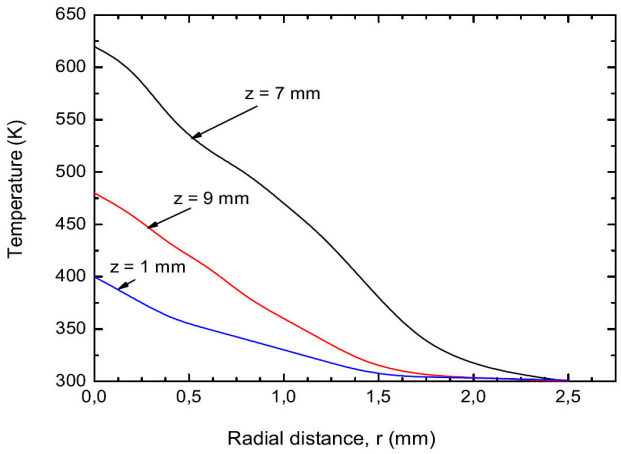

FIGURE 8. Radial evolution of neutral temperature of gas N_2.

density of the neutrals rapidly increases; a fairly large central area with a lower density increase; and the edge of the discharge where the density remains globally constant. However the radial evolution of the population is different for the two types unloaded. However, this depopulation is stronger in the case of positive discharge as soon as we move away from the exe. The maximum depopulation is one-third of the interelectrode distance.

4.2. Temperature evolution

The determination of the refractive index of the N_2 medium created by the discharge allows us to deduce not only the density of the neutral particles but also the temperature of the neutral gas. In Fig. 7 we show the axial evolution of the temperature values at different distances in the core region of the discharge for positive and negative corona discharges.

The most important concern in Fig. 7 shows that in both positive and negative coronas, the temperature value increases with z until a maximum values is reached at $z \simeq 5.3$ mm, where it starts to decrease. The temperature rise is due to conversion of electric energy into heat by the Joul's principle. It is clear that the distribution of temperatures

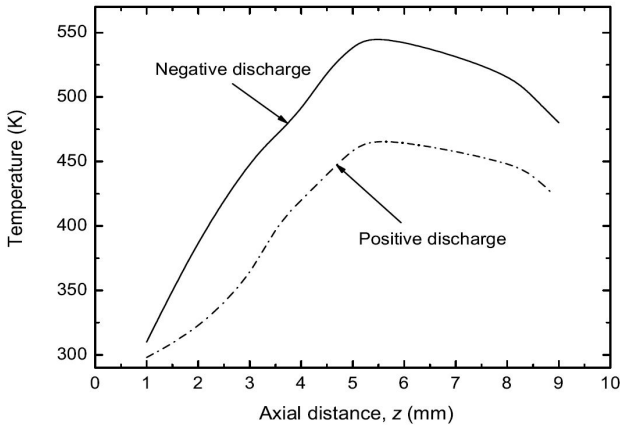

FIGURE 7. Axial evolution of neutral temperature of gas N_2.

along the axis is somewhat different in the two cases of discharge as in the case of the distribution of the density of neutral particles. Temperature variations along the axis in the case of negative discharge are greater.

Figure 8 shows the radial evolution of the neutral temperature for the positive corona discharge, for three selected values of the axial distance (*i.e.* $z = 1$, $z = 7$ and $z = 9$ mm). The maximum temperature is $\theta \simeq 624$ K at $z = 7$ mm from the point. The radial decrease in temperature is regular. Comparing this figure with the figure giving the spatial evolution of the density of neutrals, it is clear that the maximum temperature and the minimum density are located at the same point of the axis of the interelectrode space. The decrease in temperature, when we move away from the axis, is also much slower. We observe a kind of 1 mm long bearing where the temperature remains generally constant a with the positive discharge depopulation curves.

It can be seen from Fig. 8, in the low radial distance range $0 \lesssim r \lesssim 0.7$ mm when setting $z = 1$ mm, the temperature is high but decreases rapidly with rate of decrease close to $\sim 15\%$. When the distance increases, for example, z= 7 mm the temperature is high but decreases rapidly with rate of decrease around $\sim 62\%$. With increasing radial distance (i.e. intermediate rang) $0.7 \lesssim r \lesssim 1.7$ mm, for example, when setting $z = 1$ mm where the temperature decreases less rapidly with rate of decrease close to $\sim 25\%$. In the same interval at $z = 9$ mm, the temperature decreases less rapidly with rate of decrease around $\sim 26\%$. It can also be noticed from Fig. 8 that in the interval $2 \leq r \leq 2.5$ mm, the temperature remains almost constant equal to the ambient temperature (*i.e.* $\theta \approx 300$ K), and this happens whatever the values of z.

5. Conclusion

By comparing the evolution of the neutral distribution with that of the temperatures inside the landfill, we can deduce that the increase in the temperature of the gas is directly related to

the heating of the neutral by the charged particles (electronic excitation and particle collision).

Local energy transfers, charged particles−neutral particles, are not negligible even in the field of low currents. Under these high pressure conditions where electrons are highly collisional, the neutral gas no longer appears only as a source of charged particles, but also intervenes in the general dynamics of the discharge.

The interferometric diagnosis made on this positive coronal discharge, allowed us to quantitatively determine the phenomenon of depopulation of neutrals in the heart of the discharge. We have been able to deduce from the evolution of the neutrals distribution that the maximum depopulation is two-thirds of the interelectrode distance from the peak. The results obtained give values for the depopulation rate between 28 and 76%.

Acknowledgements

Pr A. K. FEROUANI gratefully acknowledges the DGRSDT, Algerian Ministry of Higher Education and Research, under Project PRFU code B00L02UN130120190002.

1. A. K. Ferouani, M. Lemerini and S. Belhour, Numerical modelling of nitrogen thermal effects produced by the negative dc corona discharge, *Plasma Science and Technology*, **12** (2010) 208. https//doi:10.1088/1009-0630/12/2/15.
2. A. K. Ferouani, M. Lemerini, L. Merad et *al.*, Numerical Modelling Point-to-Plane of Negative Corona Discharge in N_2 Under Non-Uniform Electric Field, *Plasma Science and Technology*, **17** (2015) 469. https//doi:10.1088/1009-0630/17/6/06.
3. A. Mizuno, Electrostatic precipitation *IEEE Transactions on dielectrics and electrical insulation* **7** (2000) 615. https//doi:10.1109/94.879357.
4. S. S. Grossel, Book review: Electrostatics: Principles, Problems and Applications,: J. A. Cross Adam Hilger, Bristol, U.K., 2nd Edition, 1987, pp. 491, ISBN 0 85274 599 3, *J. Loss Prevention in the Process Industries* **2** (1989) 56, https//doi.org/10.1016/0950-4230(89)87013-5.
5. C. Soria, F. Pontiga and A. Castellanos, Plasma chemical and electrical modelling of a negative DC corona in pure oxygen, *Plasma Sources Science and Technology*, **13** (2003) 95. https//doi:10.1088/0963-0252/13/1/012.
6. G. L. Rogoff, Gas Heating Effects in the Constriction of a High−*P*ressure Glow Discharge Column, *The Physics of Fluids* **15** (1972) 1931, https://doi.org/10.1063/1.1693805.
7. R. Morrow, Theory of negative corona in oxygen, *Phys. Rev. A* **32** (1985) 1799, https://doi.org/10.1103/PhysRevA.32.1799.
8. M. Lemerini, Modelisation et simulation numerique de l'empreinte thermique d'une decharge pointe-plan dans l'air. Application a l'etude de la dynamique des neutres. Tesis de doctorado, University Tlemcen-Algeria, (2001).
9. I. S. Medjahdi, A. K. Ferouani, Numerical Modeling of Impact Effect of Chemical Reactions on Nitrogen Oxide Conversion in N_2/O_2 Mixtures Under Various X%O_2 Concentrations, *IEEE Transactions on Plasma Science*, **49** (2021) 1181, https://doi.org/10.1109/TPS.2021.3059729.
10. F. Boudaoud and M. Lemerini, Using a Mach-Zehnder interferometer to deduce nitrogen density mapping, *Chinese Physics B*, **24** (2015) 075205, https://doi.org/10.1088/1674-1056/24/7/075205.
11. D. Benyahia and M. Lemerini, Interferometer method using abel inversion to deduce a mapping of helium gas density and temperature, *Microwave and Optical Technology Letters* **58** (2016) 393, https://doi.org/10.1002/mop.29578.
12. B. H. Lee *et al.*, Interferometric fiber optic sensors, *sensors*, **12** (2012) 2467, https://doi.org/10.3390/s120302467.
13. P. Lu, L. Men, K. Sooleyet and Q. Chen, Tapered fiber Mach−Zehnder interferometer for simultaneous measurement of refractive index and temperature, *Applied Physics Letters* **94** (2009) 131110, https://doi.org/10.1063/1.3115029.
14. P. V. Farrell, G. S. Springer and C. M. Vest, Heterodyne holographic interferometry: concentration and temperature measurements in gas mixtures, *Applied Optics* **21** (1982) 1624, https://doi.org/10.1364/AO.21.001624.
15. J. T. Sheridan and R. Patten, Holographic interferometry and the fractional Fourier transformation, *Optics letters*, **25** (2000) 448, https://doi.org/10.1364/OL.25.000448.
16. C. M. Vest, Holographic Interferometry, (New York: Wiley, 1979).
17. G. H. Kaufmann and C. M. Vest, Thermal waves visualized by holographic interferometry, *Applied optics*, **26** (1987) 2799, https://doi.org/10.1364/AO.26.002799.
18. P. Hariharan, Basics of interferometry, (Second Edition: Elsevier, 2010).